Arctic Amplification during the Last Glacial Inception due to a delayed response in sea ice and surface temperature

Shan Xu[1,*], Uta Krebs-Kanzow[1], Gerrit Lohmann[1,2]

[1]Alfred Wegener Institute, Helmholtz Centre for Polar and Marine Research, Klussmannstr. 3, D-27570 Bremerhaven, Germany

[2]University of Bremen, 28359 Bremen, Germany

Corresponding author: Shan Xu (shan.xu@awi.de)

Key Points:

- Our climate simulation reveals year-round cooling in the Northern Hemisphere high latitudes during the last glacial inception
- We apply a refined angular calendar for a more precise seasonal dynamics
- We identify the crucial role of albedo feedback on high-latitude radiative budget

Abstract

The last glacial inception (LGI) marks the transition from the interglacial warm climate to the glacial period with extensive Northern Hemisphere ice sheets and colder climate. This transition is initiated by decreasing summer insolation but requires positive feedbacks to stimulate the appearance of perennial snow. We perform simulations of LGI with climate model AWI-ESM-2.1, forced by the radiative and greenhouse gas forcing of 115,000 years before present. To compare with the preindustrial (PI) simulation, we use a consistent definition of the seasons during the LGI and the PI and evaluating model output on an angular astronomical calendar. Our study reveals a prominent role of sea ice in the albedo feedback to amplify the delayed climate siregnal at polar latitudes. Through a radiative budget analysis, we examine that the ice-albedo feedback exceeds the shortwave radiative forcing, contributing to the cooling and high latitude snow built-up during LGI.

Plain Language Summary

The onset of the last ice age marks the transition from the interglacial warm climate to the ice age with extensive Northern Hemisphere ice sheets and colder climate. This transition is initiated by decreasing summer irradiance and reinforced by positive feedbacks. We perform climate simulations under the radiative and greenhouse gas forcing, and use a consistent definition of seasons. Our study shows that a delayed ice-albedo feedback plays an important role in generating a cold Northern Hemisphere climate.

1 Introduction

The At the end of the last interglacial, the Earth gradually transitioned to a colder climate, the last glacial inception (LGI). Between 120-115 thousand years before present (kyr BP), snow and ice sheets started to develop in the Northern Hemisphere (NH), with ice nucleus first appearing over the Canadian Arctic islands, Labrador, northern continental Canada, continental western Siberia and Eurasian Arctic islands (Andrews and Barry, 1978; Mangerud and Svendsen, 1992; Clark et al., 1993; Svendsen et al., 2004; Lambeck et al., 2006). Different from most glacial periods, LGI is characterized by its abruptness. By 110 kyr, the ice sheets reached their maximum, covering ~70% of the area of Last Glacial Maximum (Stokes et al., 2012). Meanwhile, permanent sea ice thickened over the central Arctic and seasonal sea ice existed in the western Fram Strait (Stein et al., 2017). Planktonic and benthic foraminifera from the North Atlantic Ocean indicate that at the onset of the LGI the meridional gradient of sea surface temperature (SST) was enhanced —with very low SST at high latitudes (a cooling of around 4 K from present day; Cortijo et al., 1999) while low latitudes were slightly warmer than at present (Ruddiman and McIntyre, 1979). Although the timing of this cooling is unsynchronous and its magnitude varied globally, the northern high latitudes with a stronger and earlier cooling signal are key regions in this glaciation process.

Milankovitch (1941) postulated that the key drivers for glacial inceptions are the reduction in NH summertime insolation and the subsequent perennial snow accumulation. Previous model simulations with corresponding insolation forcing have shown a consistent cooling of temperature, an increase of snow cover and sea ice (e.g., Bahadory et al., 2021; Born et al., 2010), as also seen from proxies. However, models often fail to accurately capture the specific location, range, and expansion rate of ice sheets (e.g., Bahadory et al., 2021; Kageyama et al., 2004, Calov et al., 2005). This limits our understanding of glacial dynamics during the time period. Consequently, a key question is what positive feedbacks amplified insolation forcing during the LGI. Furthermore, it remains unclear why the high-latitude cooling is prior to other regions. In addition to insolation, other contributions have been proposed, including albedo feedbacks (Kageyama et al., 2004; Calov et al., 2005), meridional temperature gradients (Young and Bradley, 1984), North Atlantic Ocean circulation (Ruddiman and McIntyre, 1981; Imbrie et al.,1992), atmospheric circulation (Lohmann, 2017), sea ice feedback (Lachniet et al., 2017; Yoshimori et al 2002; Vavrus et al., 1999), vegetation changes (Noble et al., 1996; Gallimore and Kutzbach, 1996; Yoshimori et al., 2002; Meissner et al., 2003; Kageyama et al., 2004) etc.

Most climate simulation studies analyze their model output based on the classical "fixed-days" calendar, which cannot represent the seasonal dynamics in paleo times (e.g., Kutzbach and Gallimore, 1988; Joussaume and Braconnot, 1997; Shi et al., 2022). This approach might even lead to misinterpretations in climate patterns, such as temperature amplification, bipolar seesaw and global monsoon (Bartlein and Shafer, 2019). This bias is especially pronounced in periods like LGI. The orbital forcing during the LGI entails weak summer insolation at high latitudes on both hemispheres due to a lower-than-present obliquity and a higher-than-present eccentricity, additionally increased Earth's distance from the sun in boreal summer (like today boreal summer occurs near aphelion). The high eccentricity leads to a reduced (increased) orbital speed of the Earth around the Sun in boreal summer (winter), which, with respect to today's calendar, implies a shift of the solstices and the related seasons. Therefore, significant biases occur if we apply today's classical calendar to the seasonal cycles study of LGI.

In this paper, we conduct model simulations of PI and LGI with a coupled earth system model. By focusing on the NH high-latitude feedbacks and employing a refined astronomical calendar, we aim to bridge the gap in understanding the seasonal dynamics of paleo times, particularly the LGI.

2 Methods and Experiments

2.1 Model and experiment design

The model employed in this study is the state-of-art coupled Earth System Model AWI-ESM-2.1 (Sidorenko et al., 2019). AWI-ESM-2.1 is an atmosphere-ocean-land-sea ice model, which consists of the Finite Element Sea ice-Ocean Model FESOM-2.0 (Danilov et al., 2017; Scholz et al., 2019) and ECHAM-6.3 for the atmosphere, vegetation and land surface (Stevens et al., 2013). The coupling between FESOM and ECHAM is achieved via the parallel OASIS3-MCT coupler (Valcke, 2013). The timestep of ECHAM is 450 seconds and the FESOM timestep is 30 minutes, and the ocean and atmosphere are coupled every 6 hours via the OASIS3-MCT coupler. ECHAM was run at T63 spectral resolution with 47 vertical levels. The ocean model FESOM uses an unstructured mesh CORE-II, with resolution varying from nominal one degree in the interior of the ocean to 1/3 degree in the equatorial belt and 24 km north of 50°N (Sidorenko et al. 2019). This model has been evaluated in terms of its mean state and long-term drift under PI forcing and is proved to have good capability of modelling the main characteristics in the atmosphere and ocean (Sidorenko et al., 2019). AWI-ESM has also been successfully applied for different paleoclimate periods (Shi and Lohmann, 2016; Shi et al., 2020, 2022 a-b).

To understand the feedbacks in LGI, we conducted two simulations based on the modern topography with orbital (Berger, 1978) and radiative forcing (Köhler et al., 2017) fixed at pre-industrial (ClmPI) and 115 kyr (Clm115). Both simulations run for 1200 model years. Daily output are provided for implementation of the calendar methods. The analysis presented in this study are based on the average mean of the last 50 years data from each simulation.

2.2 Calendar effect

As discussed, applying today's fixed-day calendar to paleoclimate could result in significant bias, commonly expressed as “paleo calendar effect” (Bartlein and Shafer, 2019). To address this issue, our study adopts the "fixed-angular" calendar (hereafter angular calendar), aligned more closely with the orbital variations of Earth. Angular calendar replaces the traditional fixed-day definition with angular measurements based on Earth's orbit. Each year is divided into 360°, consequently 1° corresponding to one day, each 30° to one month, and 90° to one season. This provides a more accurate representation of the real length of months and seasons in paleo times.

We use daily model output to redefine the months of the year based on the angular calendar for both ClmPI and Clm115 experiments. In the PI scenario, the redefined month lengths from January to December are 29, 30, 30, 31, 31, 31, 31, 31, 31, 30, 30, and 30 days, respectively. For 115kyr scenario, the new month lengths are 28, 28, 29, 31, 32, 33, 33, 33, 31, 30, 29, and 28 days. This indicates longer summer and shorter winter in the LGI scenario relartive to PI.

Figure 1a-b shows the annual cycle of zonal-mean changes of insolation between LGI and PI. The incoming solar radiation at the top of the atmosphere in LGI compared with PI is primarily characterized by a decreased summer insolation and an enhanced warmer insolation, resulting in a weak seasonal contrast on both hemispheres. This adjustment in the calendr method affects the analysis of seasonal insolation and temperature anomalies, as observed in our results. Under the angular calendar, seasonal contrasts and latitudinal distribution of insolation become more symmetric. For example, the dipole pattern in autumn is no longer discernable under angular calendar, which facilitates a more concise comparison between two climates. The difference of surface temperature between two cleandars, as paleo calendar effect, is shown in Fig. 2, which also shows an invisible pattern. In the following, we only show model results based on the angular calendar.

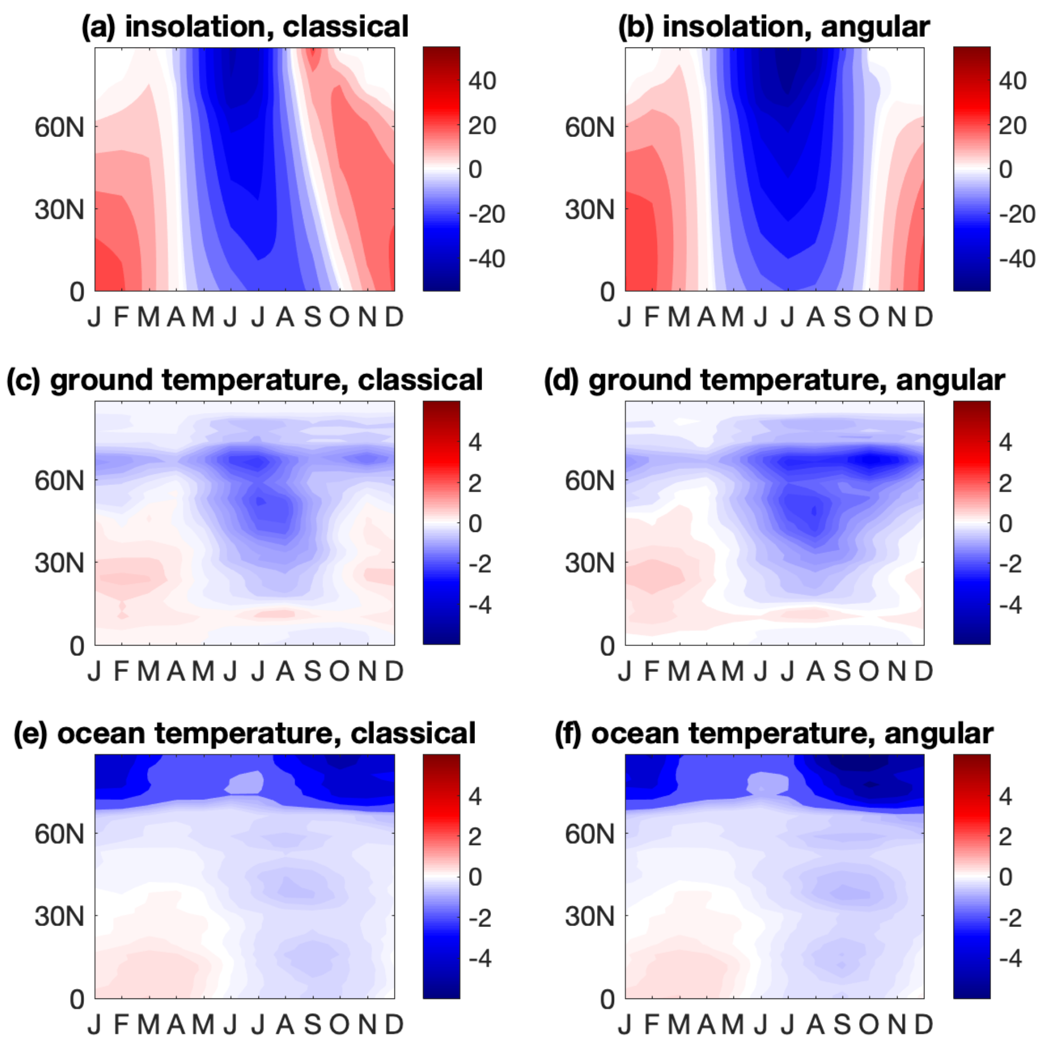

Figure 1. Annual cycle of zonal-mean changes between LGI and PI: a-b, for incoming solar radiation at the top of the atmosphere (W/m^2); c-d, for 2m temperature over land (K); e-f, for 2m temperature over ocean and sea ice-covered areas (K). Left panels use a classical fixed-day calendar. Right panels use the angular calendar.

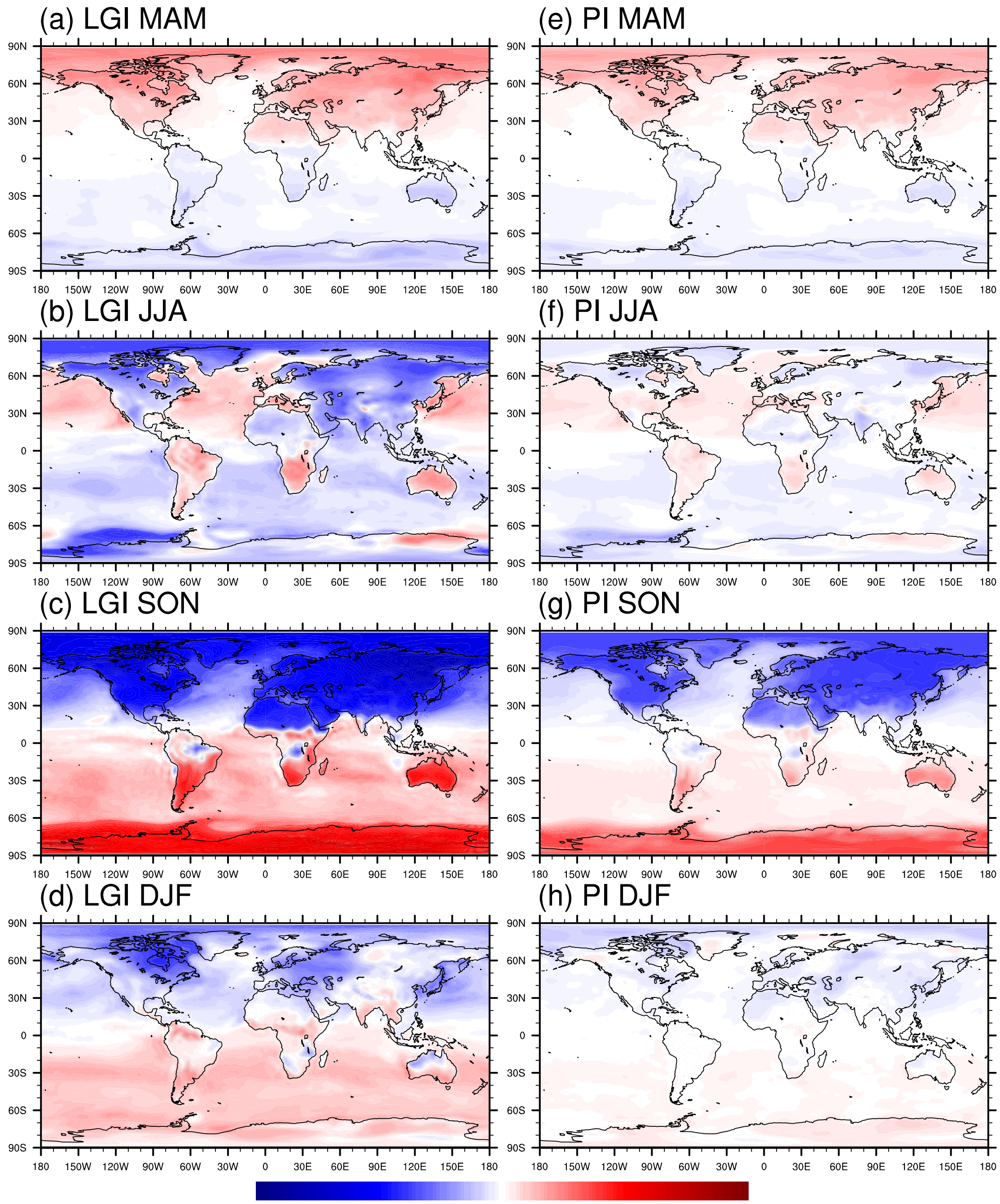

Figure 2. Paleo calendar effect on 2m temperature in K during LGI (left panel) and PI (right) in different seasons. Paleo calendar effect is defined by the anomly between augular calendar and classical calendar.

3 Results

3.1 Decoupling between insolation and temperature in the Arctic winter

As As seen from Fig. 3, the temperatures over land and ocean have a distinct response to insolation. Thus, we compare the near surface (2m) temperature over land and ocean separately.

The land temperature changes mainly follow the seasonal cycle of insolation anomalies in the low and middle latitudes with a lag of one month (Fig. 1). The minimum 2m temperature anomaly over land is seen in August with an average 0.5K cooling, while the maximum anomaly is in February with a 0.1K warming. However, at high latitudes, the temperature anomaly does not follow the seasonality of the insolation anomaly, and there is an anomalous cooling over the whole year. The zonal mean temperature north of the polar circle is about 2K colder from November to March relative to the PI, in spite of an increase of insolation in the same months across all latitudes of the NH. The minimum temperature over the Arctic realm is seen in October, delayed by two months after minimum insolation change.

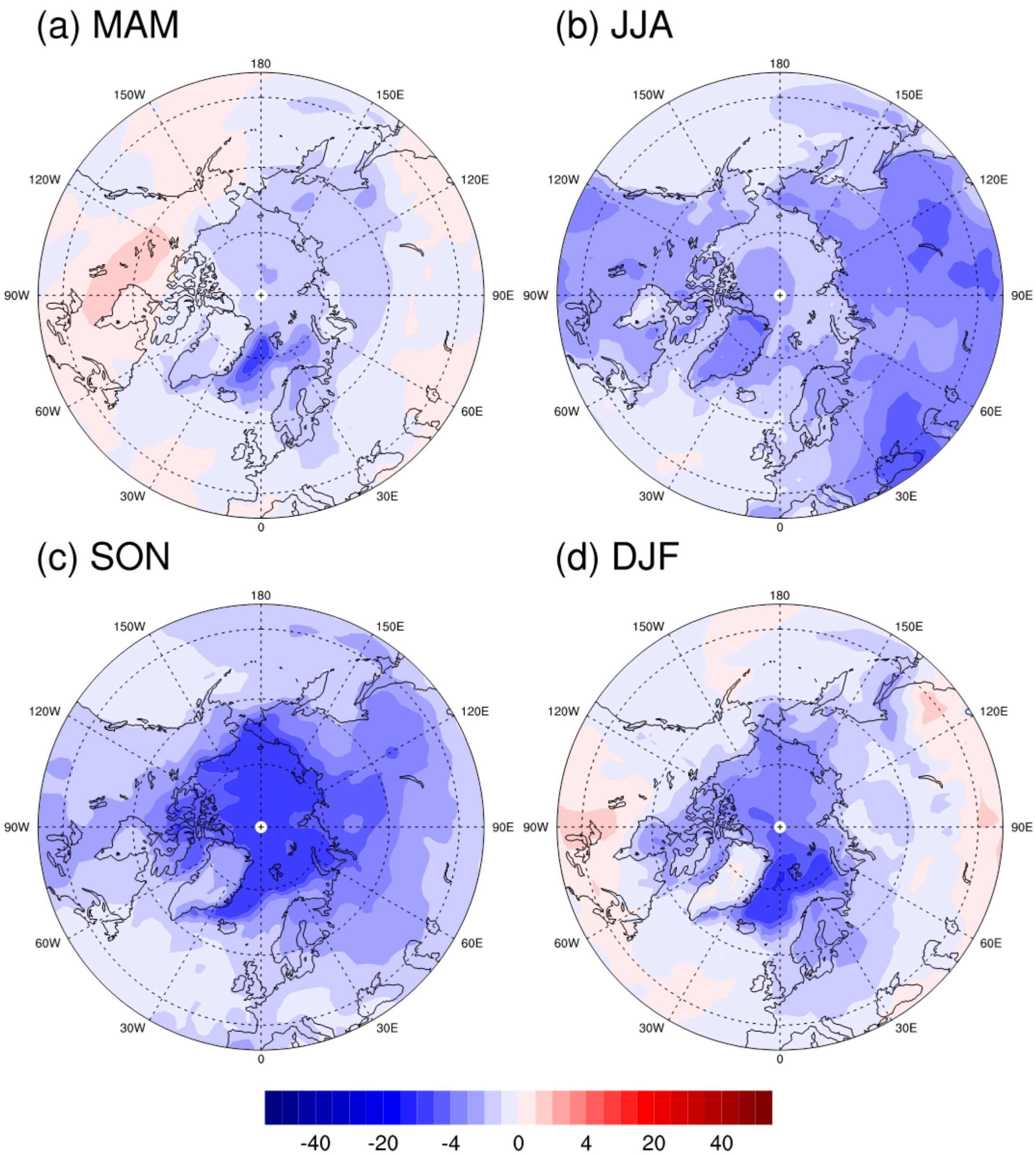

Figure 3. Near-surface 2m temperature (K) differences between LGI and PI for different seasons. Seasons are defined by the angular calendar.

SST anomalies at low latitudes and parts of mid-latitudes south of 45°N reflect the LGI insolation anomaly with warmer winters and cooler summers, but exhibit a pronounced 2-3 months seasonal lag. North of 45°N, an anomalous cooling is observed over the whole year and the minimum lags the minimum insolation by 2-4 months. North of 67°N, a remarkable Arctic cooling exceeds the decrease of temperature at mid-latitudes by about 3K in winter (October to March). This cooling closely traces sea ice edges (Fig. 4), which indicates that sea ice might play an important role on the decoupling between insolation and temperature during LGI.

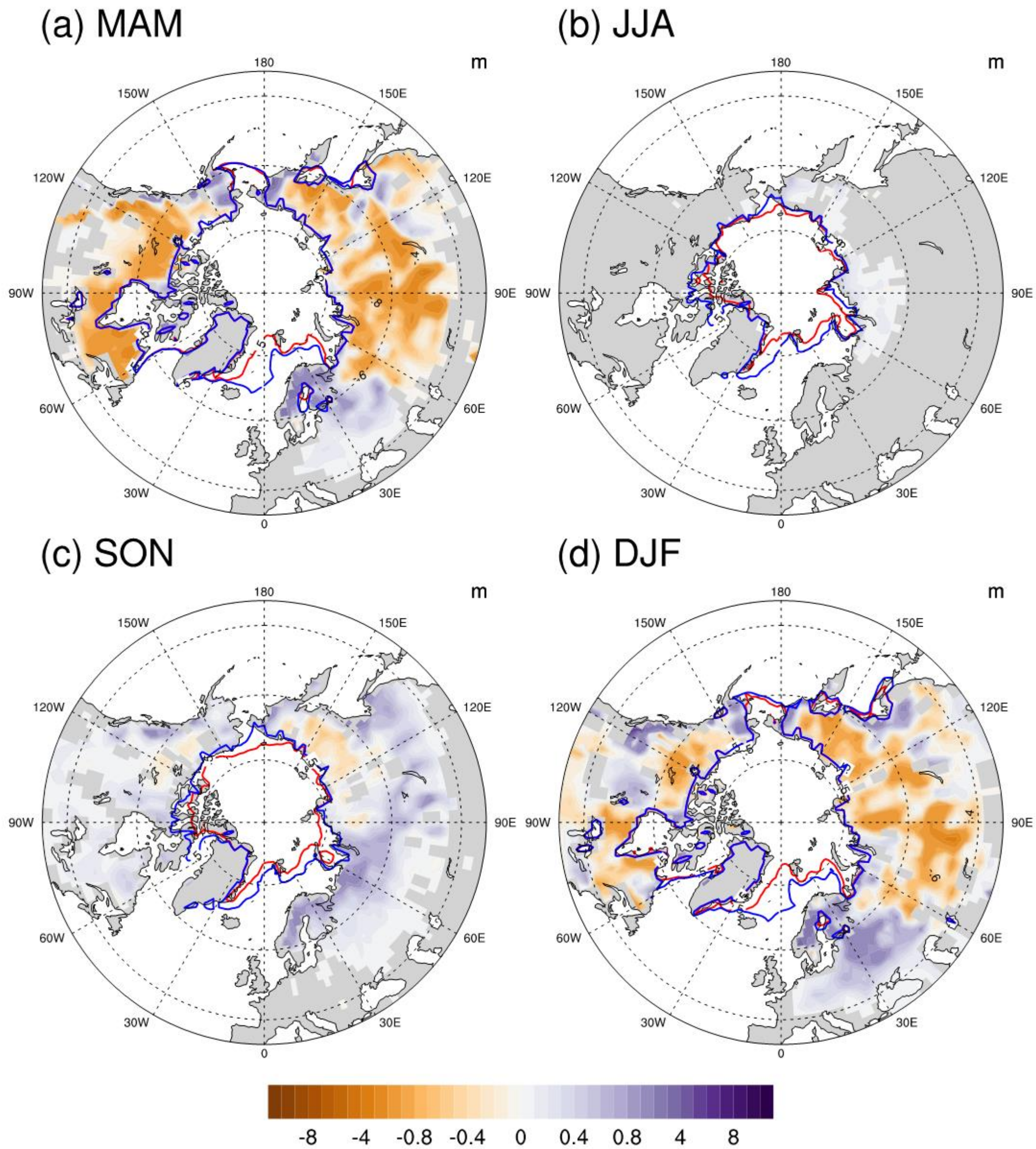

Figure 4. Snow depth and sea ice changes between LGI and PI, also in the angular calendar. Shading indicates snow depth in mm. Blue and red curves indicate areas covered by more than 50% sea ice during LGI and PI, respectively.

3.2 The sea ice and snow response

The Arctic sea ice and the continental snow cover also show strong seasonal signatures. A strong reduction in summer insolation results in increased snow accumulation and increased sea ice formation in most parts of the NH (Fig. 4). Compared to PI, increased snow in springtime at LGI is seen in Nunavut, eastern Quebec, and small regions on Baffin Island, Scandinavia, and north-eastern Siberia. These are regions where large ice caps and glaciers have been formed during this period according to ice sheet reanalysis data (Batchelor et al., 2019). Sea ice becomes thicker and covers a larger area in summer. In Clm115, the contour of 50% sea ice cover fraction extends toward the coasts in the Canadian Arctic and East Siberia Sea and shifts toward lower latitudes in the Bering Strait and Norwegian Sea. In the following autumn and winter, the less pronounced melt season further facilitates the formation of sea ice. In October, the Arctic sea-ice area anomaly reaches its maximum, concurrent and spatially correlated with the lowest Arctic temperature anomalies. However, the Norwegian Sea and western Barents Sea remain mostly ice free throughout the year in both experiments, which might be associated with a vigorous North Atlantic Current (Born et al., 2010).

3.3 Radiative budget analysis

In order to understand the relative contribution of radiative forcing on climate change, we analyze the energy budget of the Earth's surface from shortwave radiation by separating forcing and feedback components. For a given phase of the seasonal cycle, the surface shortwave radiation budget is

$$S_{snet} = S_{sd} * (1 - A) \qquad \text{Eq (1)}$$

where S_{snet} is the net surface shortwave radiation, S_{sd} is the surface downward shortwave radiation, and A is the surface albedo. These variables can also be represented as climatological mean from a common reference and their corresponding anomalies with respect to this reference. In this way, the LGI anomaly in S_{snet} can be expressed as

$$S'_{snet} = S'_{sd} * (1 - \bar{A}) - \overline{S_{sd}} * A' - S'_{sd} * A' \qquad \text{Eq (2)}$$

where the overbar indicates the climatological mean under PI and the primed quantities represent the anomalies between LGI and PI. The anomaly of S_{snet} is decomposed into three terms. The first term on the right hand side is the shortwave radiative forcing, which is the effect of the anomalous radiation without any feedbacks. The second term stands for the radiative feedback resulting from albedo changes that modify the surface radiation budget. The third term on the right hand is the residual term, including nonlinear processes resulting from the combined effect of surface radiation anomalies and albedo anomalies. Here, we call the above three terms surface radiative forcing, albedo feedback, and residual effect in our later discussion.

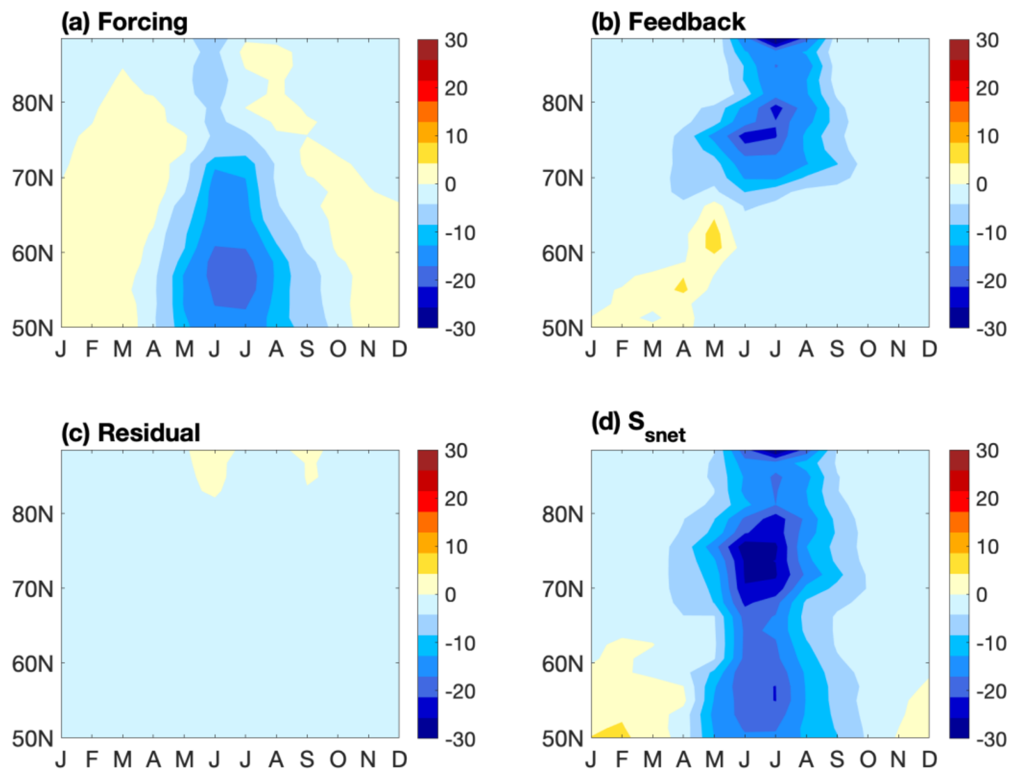

Figure 5. Results from the shortwave radiation budget analysis. a-d shows annual cycle of zonal mean surface radiative forcing, albedo feedback, residual effect, and the anomaly of net surface shortwave radiation, unit in W/m^2.

Our radiation budget analysis follwows Jackson and Broccoli (2003). The only difference is in distinguishing of the mean and variation of quantities. In their work, they determined the overbar as a long-term mean and the primed quantities as the anomaly regarding the mean value. To have a direct comparison with the profile of incoming insolation and temperature, we integrate Eq (2) zonally over both land and ocean areas. Fig. 5 shows the latitudinal profile of all the decomposition components on the right hand side of Eq (2). The surface shortwave radiative forcing decreases the most at ~55° N in summer, whereas changes in wintertime are relatively small. In higher latitudes, the albedo feedback overwhelms the weak radiative forcing due to the pronounced difference in summer sea ice coverage: forcing only contributes less than -5 W/m^2 to the total budget, while the feedback amounts to up to -30 W/m^2, resulting in a significant reduction of net surface radiation during May to September (MJJAS).

In contrast to higher latitudes on the NH, the albedo feedback is not a factor south of $67°N$, where summer sea ice does not exist during both periods. The magnitude of the residual term is much smaller than the other two terms, indicating that the combined effect from both shortwave radiative forcing and albedo feedback has a negligible contribution to the total radiation budget.

4 Discussion

We apply the coupled climate model AWI-ESM to study the mechanisms of regional cooling during the LGI. The LGI simulation exhibits a weakened seasonal cycle in temperature with the Arctic being colder than PI throughout the year. Through a radiative budget analysis, we find that in high latitudes albedo feedback exceeds the shortwave radiative forcing, contributing to the cooling in high latitude regions during the LGI, which favours a “glaciation-friendly climate” at that time.

It is interesting to discuss the geological evidences of the high-latitude climate of the LGI. During the transition from the last interglacial to the inception, the sea-ice cover was indeed quite variable (Stein et al., 2017; Kremer et al., 2018). During the early mid part of the last interglacial, sediments show a reduction in sea ice which might have been even less extensive than today (Irvali et al., 2016; Nieuwenhove et al., 2011; Kremer et al., 2018; Stein et al., 2017). During the late part of last interglacial and the transition to LGI, a major ice sheet advance is observed in the western continental margin of Svalbard (Mangerud et al., 1996, 1998) and an extended sea-ice cover at the northern and western Barents Sea continental margin (Kremer et al., 2018; Stein et al., 2017). This agrees with our model simulations on LGI showing an extended sea-ice cover relative to PI. In addition, the response of snow in our simulations also shows favorable glaciation conditions. Snow over Siberia and Canadian Arctic Islands shows longer survival time at LGI. Increased snow corresponds well with the regions where large ice caps and glaciers have been formed during the inception period (Batchelor et al, 2020). The changes on sea ice and snow variability strongly influence the radiation budget through albedo feedback over the entire Arctic and thereby have a significant impact on the temperature.

Previous model studies found that the distribution of sea ice under PI conditions and its sensitivity to different forcing is highly model dependent (Kageyama et al., 2020). In particular, unlike other models, AWI-ESM does not exhibit pronounced permanent sea ice in the Baffin and Hudson Bay, which could imply that the sensitivity of the high latitude North America is also model dependent, especially considering that more sea ice in the Baffin Bay might have an effect on the climate on the North America continent. Therefore, the spatial fingerprint of our result demonstrates that sea ice has a strong amplifying effect on the regional climate response.

Although our model simulates a longer snow season and an extended snow cover in LGI, no increased snow cover is detected in mainland Canada, particularly in eastern Quebec, which is also a potential inception location from geological data (Clark et al., 1993). Previous model studies proposed that ice nucleation first appears on high latitudes and high altitudes area, and then spreads out from these regions during LGI (Bahadory et al, 2021). The lack of permanent snow and ice cover in Quebec might be due to unresolved topography. Climate models with a higher resolution could better resolve high mountains regions, resulting in a better representation of permanent snow cover and a stronger ice-albedo feedback (Calov et al., 2005; Vavrus et al., 2011). This might be improved by applying an appropiate downscaling process that takes into account the sub-grid orography (Marshall and Clarke, 1999; Krebs-Kanzow et al., 2021).

5 Conclusions

We analyze our climate model AWI-ESM for LGI and PI conditions. Our main findings are:

a) The LGI shows a more "glaciation-friendly climate" compared to PI: a year-round NH anomalous cooling and a delayed temperature signal in response to insolation through sea ice.

b) The positive effect of albedo dominates the radiative budget on NH high latitudes, associated to expanded sea ice and snow cover. This is consistent with proxy indicators.

c) A paleo-calendar based on fixed-angular is recommended for studying seasonal paleoclimate, especially if eccentricity and precession are different from present.

A logical next step is to investigate a coupled ice sheet-climate model (e.g., Ackermann et al., 2020) in a transient mode starting from the last interglacial to investigate the feedbacks identified here.

Acknowledgments

Shan Xu is funded by the China Scholarship Council (CSC). Uta Krebs-Kanzow and Gerrit Lohmann acknowledge the Helmholtz Climate Initiative REKLIM (Regional Climate Change), Bundesministerium für Bildung und Forschung (PalMod project) and the PoF IV "Changing Earth – Sustaining our Future" research program of the Alfred Wegener Institute.

Open Research

Data for this research are available in 10.5281/zenodo.10425117. Software for this research is available in Shi et al. (2022b).

References

Ackermann, L., C. Danek, P. Gierz, and G. Lohmann (2020), AMOC Recovery in a multicentennial scenario using a coupled atmosphere-ocean-ice sheet model, *Geophysical Research Letters*, *47*(16), e2019GL086810.

Andrews, J., and R. Barry (1978), Glacial inception and disintegration during the last glaciation, *Annual Review of Earth and Planetary Sciences*, *6*(1), 205-228.

Bahadory, T., L. Tarasov, and H. Andres (2021), Last glacial inception trajectories for the Northern Hemisphere from coupled ice and climate modelling, *Climate of the Past*, *17*(1), 397-418.

Bartlein, P. J., and S. L. Shafer (2019), Paleo calendar-effect adjustments in time-slice and transient climate-model simulations (PaleoCalAdjust v1. 0): Impact and strategies for data analysis, *Geoscientific Model Development*, *12*(9), 3889-3913.

Berger, A. (1978), Long-term variations of daily insolation and Quaternary climatic changes, *Journal of Atmospheric Sciences*, *35*(12), 2362-2367.

Born, A., K. H. Nisancioglu, and P. Braconnot (2010), Sea ice induced changes in ocean circulation during the Eemian, *Climate dynamics*, *35*, 1361-1371.

Calov, R., A. Ganopolski, M. Claussen, V. Petoukhov, and R. Greve (2005a), Transient simulation of the last glacial inception. Part I: glacial inception as a bifurcation in the climate system, *Climate Dynamics*, *24*, 545-561.

Calov, R., A. Ganopolski, V. Petoukhov, M. Claussen, V. Brovkin, and C. Kubatzki (2005b), Transient simulation of the last glacial inception. Part II: sensitivity and feedback analysis, *Climate Dynamics*, *24*, 563-576.

Clark, P., J. Clague, B. B. Curry, A. Dreimanis, S. Hicock, G. Miller, G. Berger, N. Eyles, M. Lamothe, and B. Miller (1993), Initiation and development of the Laurentide and Cordilleran ice sheets following the last interglaciation, *Quaternary Science Reviews*, *12*(2), 79-114.

Cortijo, E., S. Lehman, L. Keigwin, M. Chapman, D. Paillard, and L. Labeyrie (1999), Changes in meridional temperature and salinity gradients in the North Atlantic Ocean (30–72 N) during the last interglacial period, *Paleoceanography*, *14*(1), 23-33.

Crowley, T. J. (1984), Atmospheric circulation patterns during glacial inception: A possible candidate, *Quaternary Research*, *21*(1), 105-110.

Danilov, S., D. Sidorenko, Q. Wang, and T. Jung (2017), The finite-volume sea ice–ocean model (fesom2), *Geoscientific Model Development*, *10*(2), 765-789.

De Noblet, N. I., I. C. Prentice, S. Joussaume, D. Texier, A. Botta, and A. Haxeltine (1996), Possible role of atmosphere-biosphere interactions in triggering the Last Glaciation, *Geophysical Research Letters*, *23*(22), 3191-3194.

Gallimore, R., and J. Kutzbach (1996), Role of orbitally induced changes in tundra area in the onset of glaciation, *Nature*, *381*(6582), 503-505.

Imbrie, J., E. Boyle, S. Clemens, A. Duffy, W. Howard, G. Kukla, J. Kutzbach, D. Martinson, A. McIntyre, and A. Mix (1992), On the structure and origin of major glaciation cycles 1. Linear responses to Milankovitch forcing, *Paleoceanography*, *7*(6), 701-738.

Irvalı, N., U. S. Ninnemann, H. K. F. Kleiven, E. V. Galaasen, A. Morley, and Y. Rosenthal (2016), Evidence for regional cooling, frontal advances, and East Greenland Ice Sheet changes during the demise of the last interglacial, *Quaternary Science Reviews*, *150*, 184-199.

Jackson, C., and A. Broccoli (2003), Orbital forcing of Arctic climate: mechanisms of climate response and implications for continental glaciation, *Climate Dynamics*, *21*, 539-557.

Joussaume, S., and P. Braconnot (1997), Sensitivity of paleoclimate simulation results to season definitions, *Journal of Geophysical Research: Atmospheres*, *102*(D2), 1943-1956.

Kageyama, M., S. Charbit, C. Ritz, M. Khodri, and G. Ramstein (2004), Quantifying ice-sheet feedbacks during the last glacial inception, *Geophysical Research Letters*, *31*(24).

Kageyama, M., L. C. Sime, M. Sicard, M.-V. Guarino, A. de Vernal, D. Schroeder, R. Stein, I. Malmierca-Vallet, A. Abe-Ouchi, and C. Bitz (2020), A multi-model CMIP6 study of Arctic sea ice at 127 ka: Sea ice data compilation and model differences, *Climate of the Past Discussions, 2020*, 1-33.

Köhler, P., C. Nehrbass-Ahles, J. Schmitt, T. F. Stocker, and H. Fischer (2017), A 156 kyr smoothed history of the atmospheric greenhouse gases CO 2, CH 4, and N 2 O and their radiative forcing, *Earth System Science Data*, *9*(1), 363-387.

Krebs-Kanzow, U., P. Gierz, C. B. Rodehacke, S. Xu, H. Yang, and G. Lohmann (2021), The diurnal Energy Balance Model (dEBM): a convenient surface mass balance solution for ice sheets in Earth system modeling, *The Cryosphere*, *15*(5), 2295-2313.

Kutzbach, J., and R. Gallimore (1988), Sensitivity of a coupled atmosphere/mixed layer ocean model to changes in orbital forcing at 9000 years BP, *Journal of Geophysical Research: Atmospheres*, *93*(D1), 803-821.

Lachniet, M., Y. Asmerom, V. Polyak, and R. Denniston (2017), Arctic cryosphere and Milankovitch forcing of Great Basin paleoclimate, *Scientific Reports*, *7*(1), 12955.

Lambeck, K., A. Purcell, S. Funder, K. H. Kjaer, E. Larsen, and P. Moller (2006), Constraints on the Late Saalian to early Middle Weichselian ice sheet of Eurasia from field data and rebound modelling, *Boreas*, *35*(3), 539-575.

Lohmann, G. (2017), Atmospheric bridge on orbital time scales, *Theoretical and Applied Climatology*, *128*, 709-718.

Mangerud, J., and J. I. Svendsen (1992), The last interglacial-glacial period on Spitsbergen, Svalbard, *Quaternary Science Reviews*, *11*(6), 633-664.

Mangerud, J., E. Jansen, and J. Y. Landvik (1996), Late Cenozoic history of the Scandinavian and Barents Sea ice sheets, *Global Planet Change*, *12*(1-4), 11-26.

Mangerud, J., T. Dokken, D. Hebbeln, B. Heggen, Ó. Ingólfsson, J. Y. Landvik, V. Mejdahl, J. I. Svendsen, and T. O. Vorren (1998), Fluctuations of the Svalbard–Barents Sea Ice Sheet during the last 150 000 years, *Quaternary Science Reviews*, *17*(1-3), 11-42.

Marshall, S., and G. Clarke (1999), Ice sheet inception: subgrid hypsometric parameterization of mass balance in an ice sheet model, *Climate Dynamics*, *15*, 533-550.

Meissner, K., A. Weaver, H. Matthews, and P. Cox (2003), The role of land surface dynamics in glacial inception: a study with the UVic Earth System Model, *Climate Dynamics*, *21*, 515-537.

Milankovitch, M. K. (1941), Kanon der Erdbestrahlung und seine Anwendung auf das Eiszeitenproblem, *Royal Serbian Academy Special Publication*, *133*, 1-633.

Ruddiman, W., and A. McIntyre (1979), Warmth of the subpolar North Atlantic Ocean during Northern Hemisphere ice-sheet growth, *Science*, *204*(4389), 173-175.

Shi, X., and G. Lohmann (2016), Simulated response of the mid-Holocene Atlantic meridional overturning circulation in ECHAM6-FESOM/MPIOM, *Journal of Geophysical Research: Oceans*, *121*(8), 6444-6469.

Shi, X., G. Lohmann, D. Sidorenko, and H. Yang (2020), Early-Holocene simulations using different forcings and resolutions in AWI-ESM, *The Holocene*, *30*(7), 996-1015.

Shi, X., M. Werner, Q. Wang, H. Yang, and G. Lohmann (2022a), Simulated mid-Holocene and last interglacial climate using two generations of AWI-ESM, *Journal of Climate*, *35*(23), 7811-7831.

Shi, X., M. Werner, C. Krug, C. M. Brierley, A. Zhao, E. Igbinosa, P. Braconnot, E. Brady, J. Cao, and R. d'Agostino (2022b), Calendar effects on surface air temperature and precipitation based on model-ensemble equilibrium and transient simulations from PMIP4 and PACMEDY, *Climate of the Past*, *18*(5), 1047-1070.

Sidorenko, D., H. F. Goessling, N. Koldunov, P. Scholz, S. Danilov, D. Barbi, W. Cabos, O. Gurses, S. Harig, and C. Hinrichs (2019), Evaluation of FESOM2. 0 coupled to ECHAM6. 3: preindustrial and HighResMIP simulations, *Journal of Advances in Modeling Earth Systems*, *11*(11), 3794-3815.

Stein, R., K. Fahl, P. Gierz, F. Niessen, and G. Lohmann (2017), Arctic Ocean sea ice cover during the penultimate glacial and the last interglacial, *Nature communications*, *8*(1), 373.

Stevens, B., M. Giorgetta, M. Esch, T. Mauritsen, T. Crueger, S. Rast, M. Salzmann, H. Schmidt, J. Bader, and K. Block (2013), Atmospheric component of the MPI-M earth system model: ECHAM6, *Journal of Advances in Modeling Earth Systems*, *5*(2), 146-172.

Stokes, C. R., L. Tarasov, and A. S. Dyke (2012), Dynamics of the North American Ice Sheet Complex during its inception and build-up to the Last Glacial Maximum, *Quaternary Science Reviews*, *50*, 86-104.

Svendsen, J. I., H. Alexanderson, V. I. Astakhov, I. Demidov, J. A. Dowdeswell, S. Funder, V. Gataullin, M. Henriksen, C. Hjort, and M. Houmark-Nielsen (2004), Late Quaternary ice sheet history of northern Eurasia, *Quaternary Science Reviews*, *23*(11-13), 1229-1271.

Valcke, S. (2013), The OASIS3 coupler: A European climate modelling community software, *Geoscientific Model Development*, *6*(2), 373-388.

Van Nieuwenhove, N., H. A. Bauch, F. Eynaud, E. Kandiano, E. Cortijo, and J.-L. Turon (2011), Evidence for delayed poleward expansion of North Atlantic surface waters during the last interglacial (MIS 5e), *Quaternary Science Reviews*, *30*(7-8), 934-946.

Vavrus, S., G. Philippon-Berthier, J. E. Kutzbach, and W. F. Ruddiman (2011), The role of GCM resolution in simulating glacial inception, *The Holocene*, *21*(5), 819-830.

Vavrus, S. J. (1999), The response of the coupled arctic sea ice–atmosphere system to orbital forcing and ice motion at 6 kyr and 115 kyr BP, *Journal of Climate*, *12*(3), 873-896.

Yoshimori, M., M. Reader, A. Weaver, and N. McFarlane (2002), On the causes of glacial inception at 116 kaBP, *Climate Dynamics*, *18*, 383-402.

Young, M., and R. Bradley (1984), Insolation gradients and the paleoclimatic record, in *Milankovitch and Climate: Understanding the Response to Astronomical Forcing*, edited, pp. 707-713, Springer.